THE JOURNAL OF PHYSICAL CHEMISTRY B

Article

pubs.acs.org/JPCB

Simulating the Dynamics and Orientations of Spin-Labeled Side Chains in a Protein–DNA Complex

Jessica L. Sarver,[†] Jacqueline E. Townsend,[‡] Gayathri Rajapakse,[†] Linda Jen-Jacobson,[‡] and Sunil Saxena*,[†]

[†]Department of Chemistry, University of Pittsburgh, 219 Parkman Avenue, Pittsburgh, Pennsylvania 15260, United States

[‡]Department of Biological Sciences, University of Pittsburgh, 4249 Fifth Avenue, Pittsburgh, Pennsylvania 15260, United States

Supporting Information

ABSTRACT: Site-directed spin labeling, wherein a nitroxide side chain is introduced into a protein at a selected mutant site, is increasingly employed to investigate biological systems by electron spin resonance (ESR) spectroscopy. An understanding of the packing and dynamics of the spin label is needed to extract the biologically relevant information about the macromolecule from ESR measurements. In this work, molecular dynamics (MD) simulations were performed on the spin-labeled restriction endonuclease, *Eco*RI in complex with DNA. Mutants of this homodimeric enzyme were previously constructed, and distance measurements were performed using the double electron electron resonance experiment. These correlated distance constraints have been leveraged with MD simulations to learn about side chain packing and preferred conformers of the spin label on sites in an α-helix and a β-strand. We found three dihedral angles of the spin label side chain to be most sensitive to the secondary structure where the spin label was located. Conformers sampled by the spin label differed between secondary structures as well. C_α–C_α distance distributions were constructed and used to extract details about the protein backbone mobility at the two spin labeled sites. These simulation studies enhance our understanding of the behavior of spin labels in proteins and thus expand the ability of ESR spectroscopy to contribute to knowledge of protein structure and dynamics.

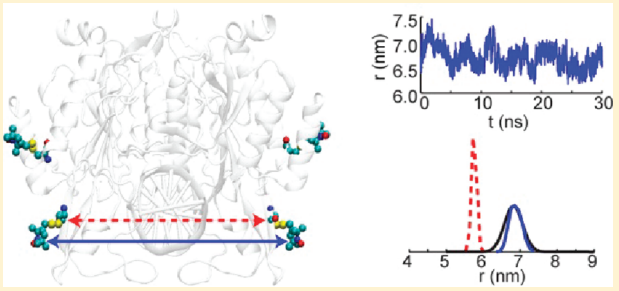

INTRODUCTION

Site-directed spin labeling (SDSL) for electron spin resonance (ESR) spectroscopy has now become a widely utilized method to obtain structural constraints, probe conformational changes, and monitor protein–protein and protein–ligand interactions.[1,2] In such experiments, the presence of the spin label contributes substantially to the experimental observables. The inherent mobility of the spin label side chain contributes to the dynamics measured in the continuous wave (CW) spectral line shape. Furthermore, the length of the spin label adds to the distance constraints that are measured most commonly using the pulsed double electron electron resonance (DEER) experiment.[3,4] Ultimately, the position and mobility of the *backbone* are sought when performing ESR distance and dynamics measurements on biological systems or nanostructures. For this reason, work has progressed toward deconvoluting the backbone and spin label effects on such measurements through experiment and simulation.

The DEER experiment has been utilized to probe the flexibility and orientations of terminally spin-labeled oligomers [bis-peptides or oligo(para-phenyleneethynylene)s] by analysis of orientational effects[5] and distance distribution functions.[6] Molecular models have also been developed to more accurately extract backbone details of these oligomers.[7−9] In these models, parameters describing the orientation and flexibility of each segment with respect to subsequent segments of the oligomer were optimized such that the simulated distance distributions agreed with experiment. From these studies, end-to-end distance distributions from the oligomer backbone could be extracted, providing insight into the shape and flexibilities of these structures.

To resolve the backbone details for larger systems, such as peptides and proteins, a systematic understanding of the spin label conformation and packing as well as dynamics is needed. The behavior of the spin label has been probed in various systems by a number of methods, including X-ray crystallography,[10−17] ab initio calculation,[18−20] rotamer libraries,[21−23] as well as molecular dynamics (MD)[24−31] and Monte Carlo simulations.[32−35] Using X-ray crystallography, Hubbell and coworkers determined preferred conformations of the spin label side chain at solvent-accessible helical and loop sites in T4 lysozyme.[11,12,14] The spin label conformation can be defined by five dihedral angles (χ_1–χ_5) along the length of the spin label side chain. These angles are represented on the spin label in Figure 1A. These analyses suggest that for solvent-accessible, noninteracting spin-labeled sites, the internal motion of the

Received: November 17, 2011
Revised: March 6, 2012
Published: March 10, 2012

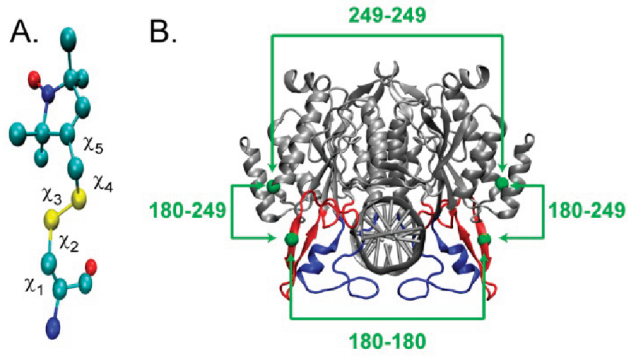

Figure 1. (A) MTSSL structure with the five defining dihedral angles, χ_1–χ_5. (B) Crystal structure of the specific *Eco*RI–DNA complex (PDB 1CKQ)[47] with residues 180 and 249 represented by green spheres. The distances measured experimentally are also shown by the arrowed brackets: 180–180, 180–249,[49] and from this work 249–249.

spin label results primarily from the rotations about the terminal dihedral angles (χ_4 and χ_5), known as the χ_4/χ_5 model. At such sites, local interactions with the backbone atoms and disulfide group of the spin label restrained the side chain such that the [χ_1, χ_2], and occasionally the disulfide bond conformations (χ_3) could be resolved. On the other hand, the nitroxide ring was rarely resolved, indicating that the χ_4 and χ_5 angles were highly unconstrained. These structures, taken together with CW-ESR data,[36,37] led to the formulation of the χ_4/χ_5 model. At sites where the spin label is involved in interactions with neighboring groups, fully resolved crystal structures of the entire nitroxide side chain were possible.[10,13,16]

Freed and co-workers[18] used the Hartree–Fock theory to calculate torsional profiles of the five defining dihedral angles of the spin label using fragments of the spin label side chain. Using the minima values from the torsional profiles, as well as steric constraints, 18 possible conformers of the spin label on a polyalanine α-helix were identified. Along these same lines, Hubbell and co-workers[19] recently utilized density functional theory (DFT) to calculate the lowest energy conformations (χ_1–χ_3) of the spin label on a peptide fragment. The conformers were then modeled on a polyglycine to identify the interactions that stabilize the conformers in a helical environment. This work differed from that of Freed and co-workers due to the inclusion of backbone atoms in the calculations. This enabled the observation of interactions between the S_δ of the spin label and backbone atoms of the peptide fragment.

Alternatively, several groups have utilized MD simulations to model spin-labeled systems comparing the simulated results to experimental CW[24−28] or DEER[29−31] results. One of the largest challenges in performing MD simulations to model the side chain conformation and dynamics is sufficient sampling. Different techniques have been employed to overcome this problem such as performing the simulations at high temperatures[25,30] or in implicit solvent.[32] Such conditions, however, can be misrepresentative of the experimental conditions to which the simulations are compared. It has been shown by others that in order to effectively model the spin label, simulations must be performed for long time scales.[20,28,29] For example, Roux and co-workers parametrized the MTS spin label and performed long MD simulations (101 ns) using 18 different starting orientations of the spin label on a polyalanine α-helix.[20]

As another means to ensure sufficient sampling of the spin label conformer space, Fajer and co-workers developed a Monte Carlo rotamer search technique.[33,34] The rotamer search used the Metropolis criterion to identify the lowest energy conformers at the spin-labeled site.[38] Subsequent MD simulations, using the lowest energy conformers as starting orientations of the spin label, enabled sampling of rotamer minima in the potential energy landscape of the spin-labeled system.[28] This technique was subsequently expanded using a simulated scaling approach to enhance the conformational sampling of the spin label during the MD production run.[39] In this method, the MD trajectory is coupled to a potential scaling parameter. A walk through the potential scaling parameter space weights the potential energy surface of the spin-labeled region. In this way, the potential energy barriers of different spin-labeled conformations could be crossed, enhancing the spin label sampling during the MD simulation.[34]

Significant insight has been gained on the preferred conformations and dynamics of the spin label from these studies. However, the majority of the in-depth analysis has been performed on spin-labeled α-helical structures. There is less information on the behavior of the spin label on other secondary structures such as a β-strand or loop region. Using the cellular retinol-binding protein (CRBP), Hubbell and co-workers performed a thorough analysis of the spin label present on β-strands.[40] The dynamics of the spin label on interior and edge strands were investigated using CW-ESR. Allowed conformations of the spin label were derived from spectral analysis and a manual variation of the spin label side chain, which was built into the crystal structure of CRBP at the various spin labeled sites. In addition, a recent crystal structure of the spin-labeled β-barrel membrane protein, BtuB, was published by Freed et al. which resolved the orientation of spin labels present on β-strands of the barrel in or adjacent to the lipid bilayer.[17] Furthermore, MD simulations of the spin label on β-strands have been used in conjunction with distance constraints to model protein structures through simulated annealing routines.[41−43] However, a detailed analysis of the preferred spin label conformers was not provided. Although these works provide initial insight, more analyses are required to further our understanding of the behavior of the spin label on β-strands.

Adding to the current understanding of the spin label conformers and dynamics may lead to general rules of packing that may enhance the ability to extract information about protein structure and function from ESR measurements. We can augment this knowledge by performing simulations on a spin-labeled protein that has been investigated experimentally. Accordingly, MD simulations were performed, and compared to experiment, to model the nitroxide spin label located on two different secondary structures of the spin-labeled *Eco*RI–DNA complex: 180 (β-strand) and 249 (α-helix). *Eco*RI is a 62 kDa homodimer restriction endonuclease that binds to and cleaves a specific six base pair sequence GAATTC in DNA. The crystal structure of the specific complex of *Eco*RI has been determined, and many thermodynamic and kinetic studies have been done to understand the extreme binding specificity of this enzyme. For instance, *Eco*RI binds with an affinity of up to 96 000-fold greater to its specific sequence than to a sequence that differs by one base pair.[44,45] The structure of *Eco*RI consists of a large, stable main domain and two arms (inner and outer) that enfold the DNA.[46,47] These arms are highlighted in Figure 1B in blue (inner) and red (outer); the main domain and DNA are silver.

dx.doi.org/10.1021/jp211094n | J. Phys. Chem. B 2012, 116, 4024–4033

This arm region is believed to play a role in the binding specificity of *Eco*RI due to key contacts made between the arms and the DNA backbone.[45,48] To shed light on this region, structural constraints were obtained by performing several distance measurements using the DEER experiment on the specific *Eco*RI−DNA complex.[49] In this work we have leveraged these correlated distance constraints with MD simulations to learn about side chain packing and dynamics of the spin label as well as backbone details at two different spin labeled sites in the *Eco*RI−DNA complex.

METHODS

DEER Experiments. Distance measurements were previously published on the methanethiosulfonate spin-labeled (MTSSL) S180C (single) and S180C−K249C (double) mutant proteins in specific *Eco*RI−DNA complexes.[49] In the current study, the DEER experiment was performed on the MTSSL-K249C mutant protein using a Bruker EleXsys CW/FT X-band ESR spectrometer with the Bruker X-band ER-MD5 resonator. The MTSSL-K249C sample was prepared in 30% deuterated glycerol, 65% deuterated water, and 5% protonated water, resulting in a final protein concentration of 180 μM. Appropriate salt concentrations (0.22 M) and pH as well as a 4:1 DNA:protein ratio was used to ensure that at least 99% of the sample existed as the protein−DNA complex.[50] The sample was flash frozen by plunging the capillary into liquid nitrogen-cooled propane. The four-pulse DEER experiment was performed at 40 K using an Oxford ITC 503 temperature controller and CF935 dynamic continuous flow cryostat. The observer $\pi/2$ and π pulses were 16 and 32 ns respectively, and the pumping pulse was 32 ns. The pump pulse was located at the maximum of the nitroxide spectrum with the observer pulse applied at a frequency ∼70 MHz higher. Deuteration of the solvent and glycerol resulted in a phase memory time of 2.5−3 μs, enabling the measurement of the long distance expected for the K249C mutant (C_α−C_α = 5.7 nm). A stepsize of 10 ns was used, and the integrated echo intensity was collected for 512 points. The pump pulse began 200 ns before the echo so that the zero time could accurately be determined. The data acquisition time was 75 h.

MD Simulations. Sites 180 and 249 on the crystal structure of the specific *Eco*RI−DNA complex[46,47] were mutated to nitroxide spin-labeled cysteines using the VMD program.[51] A Metropolis Monte Carlo minimization (MMCM) rotamer search was then performed in CHARMM[52] using the rotamer search program developed by Fajer et al.[33] Parameters describing the spin label force field were taken from the work of Sezer et al.[20] The CHARMM27 force field was used for the protein and DNA.[53] To ensure the full rotamer space of the spin label was accessed during the rotamer search, 10 rotamer searches were performed starting with different initial orientations of the spin label. Each rotamer search was performed until ∼1000−1500 conformers had been generated at each spin-labeled site. Ten of the lowest energy conformers were selected for both sites separately. Using these conformers, 10 doubly labeled (180 and 249) specific *Eco*RI−DNA complexes were constructed for MD simulation.

All structures were solvated in an explicit water box, and counterions were added to neutralize the system and provide a salt concentration comparable to experiment ([NaCl] = 0.22 M). All MD simulations were performed using the NAMD program.[54] The structures were energy minimized using a conjugate gradient method. After heating the system to 300 K, the system was equilibrated for 1 ns in an NPT ensemble of 1 atm using a Langevin piston. During both the minimization and equilibration steps, the protein backbone and DNA were restrained as well as the spin labels. Production runs were performed in an NVT ensemble for 30 ns using a 2 fs time step. Periodic boundary conditions were used, and particle mesh Ewald summation was used to treat the electrostatic interactions. To ensure reliability in the simulated results, the last 20 ns of the simulation, where the protein backbone had fully equilibrated, were used for analysis. Visualizations were done using VMD.[51]

RESULTS AND DISCUSSION

***Eco*RI DEER Measurements.** Distance measurements were previously published on the specific *Eco*RI−DNA complex to better understand the orientation and behavior of the arm region of this DNA-binding protein.[49] The *Eco*RI mutant proteins were generated as described previously[55] and spin labeled at sites 180 (β-strand, outer arm) and 249 (α-helix, main domain). Due to the homodimeric nature of *Eco*RI, spin labeling of the protein with a single cysteine mutation results in two spin-labeled sites in the DNA-bound complex. Double mutations provide four sites for labeling. The intermonomer (180−180 and 249−249) and *intra*monomer (180−249) distances that were measured are shown in Figure 1B (green brackets). The distance measurement in the outer arm (180−180) was performed to observe changes in this region upon binding to different sequences of DNA. The outer arm to main domain *intra*monomer (180−249) distance measurement provides yet another point-to-point distance to better triangulate the location of the outer arm upon binding different sequences of DNA. In principle, multiple distances corresponding to the 180−180, 249−249, and 180−249 intermonomer distances could also be detected in the 180−249 double mutant. However, the C_α−C_α distances for these intermonomer constraints are on the order of 6.0 nm and a time domain of only 1.5 μs was collected, thus such long distances were not detected. The 180−180 and 180−249 distance measurements were performed and published previously by Stone et al.[49] These distance constraints are augmented by the 249−249 intermonomer distance measured in this work. Site 249 resides in the main domain of *Eco*RI and has restricted motion. Thus the intersubunit distance between sites 249 was determined to serve as a reference for comparison to the distance information obtained for the arm region.

Both the 180−180 and 249−249 distance measurements were close to the upper limit of distances measurable by the DEER technique (C_α−C_α = 5.6 and 5.7 nm, respectively). Due to the low modulation frequency for such long distances, there is an inherent uncertainty in the background subtraction, and, subsequently, fitting of the DEER data needed to extract distance distributions from the time domain data. Using the DeerAnalysis2009[56] program, the previous fit to the 180−180 experimental data was refined. Both sets of data were fit using Gaussian distributions. The raw data and background fit for the 249−249 data is shown in Figure S3 in the Supporting Information as well as a more detailed discussion on the background correction of the data.

The background-subtracted DEER time domain signal and corresponding distance distribution for the 249−249 distance measurement are shown in Figure 2. Unexpectedly, a bimodal distribution was observed for this distance measurement. On the basis of the C_α−C_α distance from the crystal structure of

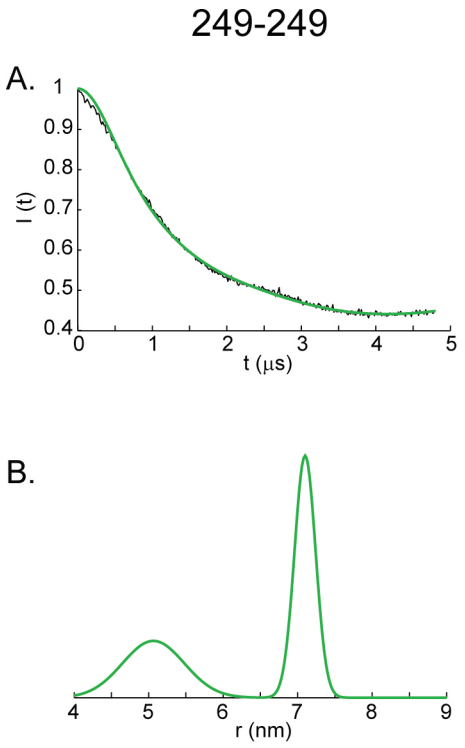

Figure 2. (A) The background subtracted time domain signal for the 249−249 intermonomer distance measurement performed using the DEER experiment. (B) The experimental distance distribution extracted from the time domain signal using DeerAnalysis2009.[56] The data was fit using two Gaussians.

the specific *Eco*RI−DNA complex (5.7 nm), the longer distance acquired (7.1 nm) is reasonable taking into account the added length of the spin label. However, a shorter distance (5.1 nm), comprising ∼40% of the distance distribution, was also observed. One possibility is that this bimodality arises from different conformers sampled by the spin label resulting in two observed distances. Such an orientation of the spin label would be unlikely, however, as it would have to protrude into the protein to achieve such a distance. Additionally, two spin label conformers would likely result in a trimodal distribution due to the combination of the spin label conformations and the distances between them.

A second possibility is that oligomerization of the *Eco*RI complex occurs in solution, such that a second, shorter intercomplex distance of 5.1 nm would be detected in our experiments. Oligomerization of *Eco*RI into a trimer of dimers has been observed in the crystal structure of the complex, and modeling (Supporting Information) with plausible assumptions suggests that this could approximately produce the observed distance. However, we do not know whether oligomerization occurs in solution under these conditions, and we are currently testing this possibility experimentally.

The possibility of oligomerization occurring in solution is further supported by the fact that the 249−249 DEER signal possesses a larger modulation depth than expected (from theoretical calculations and calibration experiments as discussed in the Supporting Information). This signifies a larger number of coupled spins than expected from just two spin labeled 249 sites in the *Eco*RI-complex, suggesting that higher order oligomers may have formed in this sample. Indeed, the modulation depth (Δ) for the 249−249 results (Δ = 0.41) is greater than that of the 180−180 results (Δ = 0.68), even though the experiments were performed under similar conditions. Ultimately, the 7.1 nm distance was primarily considered when comparing the simulated and experimental distance distributions.

MD Simulated Distance Distributions. Although the DEER data provides structural constraints in the distances between the spin labels, the backbone C_α−C_α distances and distributions are more biologically relevant to understanding the backbone structure and dynamics of *Eco*RI. To this end, MD simulations were performed on the specific *Eco*RI−DNA complex to model the spin-labeled sites that were investigated experimentally: 180 (β-strand) and 249 (α-helix). Ten independent runs with different starting spin label conformations were performed to effectively sample the spin label rotamer space and test for convergence of the individual structures to a common preferred conformer or conformers. To identify the relevant simulated data, distance distributions between the nitrogen atoms of the spin label were constructed from the MD trajectories and compared to those obtained from the DEER experiment. By using the experimental results to identify which simulations to use for further analyses, the simulations were not biased by experimental restraints, which can perturb the simulated results.[57]

Distance distributions were constructed, from all 10 parallel runs, for each of the experimentally measured distances: 180−180 intermonomer, 180−249 *intra*monomer, and 249−249 intermonomer, resulting in a total of 40 simulated distance distributions (two 180−249 *intra*monomer distances extracted from simulated results). MD runs, for which the simulated results reproduced those of the experiment, were used to draw conclusions about the backbone details of the specific *Eco*RI−DNA complex. Two criteria were used to compare the simulated and experimental results. First, agreement on the average distance and standard deviation of the experimental and simulated distance distributions was assessed. Agreement of all four distance distributions (180−180, 249−249, and *both* 180−249) with experiment was assessed simultaneously. The 180−249 *intra*monomer distance measurement was essential, as it provides a correlation between the 180−180 and 249−249 experimental results. Because of this, the conformation of the spin label must be such that not only are the 180−180 and 249−249 distance distributions in agreement with experiment, but also the 180−249 in *both* monomers. Second, the local backbone root-mean-square deviations (rmsd's) of the spin labeled sites and ∼30 surrounding residues were considered. The rmsd measures the magnitude of variation in the position of the backbone atoms from a reference point, in this case the backbone atom positions at the beginning of the 30 ns production run. Using this rmsd, the initial drift and eventual equilibration of the atom positions can be observed. Simulated results with rmsd's that are either high or continually increase throughout the simulation may depict artificial behavior of the system due to a lack of equilibration or convergence near the spin labeled site. Thus, only simulated results from stable, equilibrated runs were considered.

Of the 10 parallel simulations performed on the doubly labeled (180 and 249) system, two runs had excellent agreement with experiment (runs **i** and **ii**). In these runs, all four constraints (180−180, 249−249, and both 180−249) agreed with the respective experimental distance distributions and possessed stable local backbone rmsd's. The resultant distance distributions of these runs are presented in Figure 3

dx.doi.org/10.1021/jp211094n | J. Phys. Chem. B 2012, 116, 4024−4033

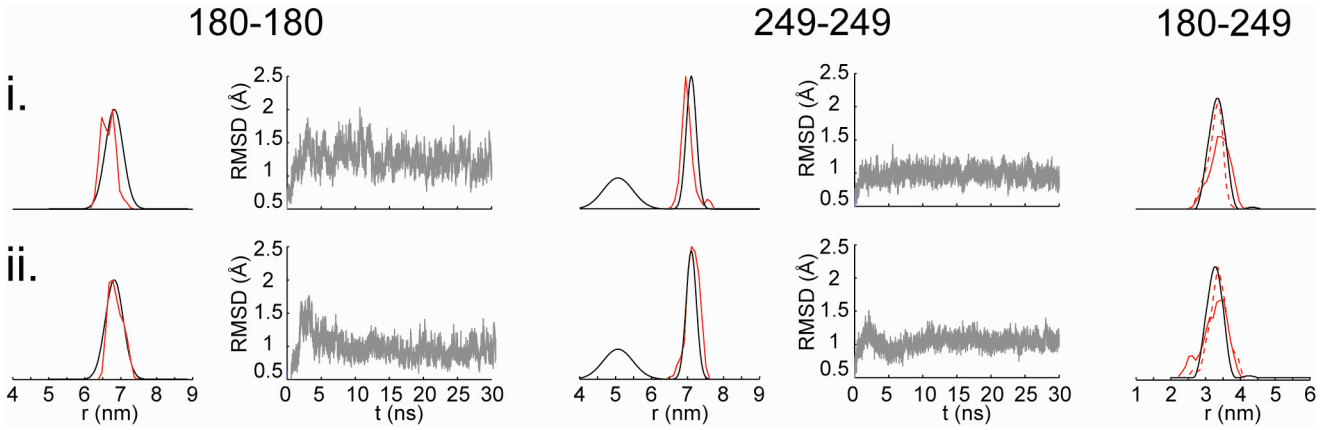

Figure 3. Comparison of the experimental[49] (black) and simulated (red) distance distributions for runs **i** and **ii**, which were found to agree with all three experimental distance constraints. The local backbone rmsd trajectories are shown for both spin labeled sites 180 and 249 (gray). The simulated 180−249 distances within the two monomers of *Eco*RI are shown as solid and dashed lines.

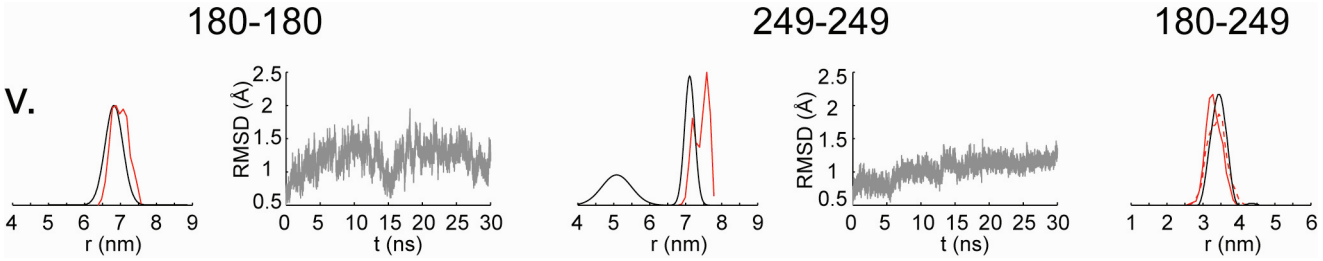

Figure 4. Comparison of the experimental[49] (black) and simulated (red) distance distributions for run **v**. The local backbone rmsd trajectories for both spin labeled sites are stable (gray); however, only the 180−180 and 180−249 simulated results agree with experiment.

where the experimental distributions are shown in black and the simulated in red. In the case of the 180−249 *intra*monomer distance distributions, two simulated results were measured, one within each monomer of the *Eco*RI-DNA complex. These are shown individually as solid or dashed red lines. The local backbone rmsd trajectories are also shown in gray for sites 180 and 249, respectively. Two of the remaining eight runs possessed unstable rmsd's even after 30 ns of simulation (runs **iii** and **iv**, Figure S1 in the Supporting Information). Of the remaining 6 runs, the rmsd's were stable; however, only two or three of the simulated distributions agreed with experiment. Run **v**, shown in Figure 4, is an example of this partial agreement between the simulated and experimental results. In this run, the 180−180 and both of the 180−249 simulated distance distributions are found to compare well with that of the experimental distribution. The 249−249 distribution, however, does not, due to a bimodal distribution (within the 7.1 nm experimental distance measurement) and an average distance larger than experiment. The remaining runs are shown in Figure S2 of the Supporting Information. Using such stringent criteria to identify the relevant simulation results increases the confidence in the data extracted from the simulations. It should be noted that in all 10 of the simulated 249−249 distance distributions, a distance corresponding to the shorter (5.1 nm) experimental distance was never observed. This supports the suggestion that a second conformation of the spin label is *not* the cause of the second, shorter experimental distance observed in the 249−249 DEER results.

MD runs that agreed with experimental data were used to extract backbone $C_\alpha-C_\alpha$ distance distributions. Figure 5 shows simulated $C_\alpha-C_\alpha$ distance distributions (blue) overlaid on the validated nitroxide−nitroxide (red) distributions. The gray dashed vertical line indicates the $C_\alpha-C_\alpha$ distance obtained from the crystal structure of the specific *Eco*RI−DNA complex. The mean $C_\alpha-C_\alpha$ 180−180, 180−249, and 249−249 distances from simulation were only 0.1−0.2 nm longer than that of the crystal structure. This small discrepancy may be attributed to the tighter packed structure of *Eco*RI in the crystalline state versus solution where the protein is more flexible and, on average, experiences larger $C_\alpha-C_\alpha$ distances.

The standard deviations of the $C_\alpha-C_\alpha$ distance distributions provided insight into the backbone mobility at the two spin-labeled sites. The standard deviations of the 180−180 $C_\alpha-C_\alpha$ distance distributions were merely 0.02 nm larger than those of the 249−249 results, indicating that the backbone at site 180 (β-strand) is slightly more mobile than at site 249 (α-helix). This similarity may be due to both spin-labeled sites being located on stable secondary structural motifs: 180 on a β-strand and 249 on an α-helix. The slight increase in the backbone mobility at site 180 may arise from the β-strand being located on the outer arm of *Eco*RI. Indeed, the rmsd values found at site 180 are slightly higher than those at site 249, contributing to the proposal that the arm region of *Eco*RI is slightly more mobile than the main domain. These results agree with the proposed order and rigidity of the main domain compared to the arm region in the crystal structure of the *Eco*RI apoenzyme.[58] CW experiments have been performed, and analyses of this data are currently underway to further investigate the dynamics of these different spin labeled sites in the *Eco*RI−DNA complex in solution.

Although there are clear differences in the nitroxide−nitroxide distributions between MD runs that agree with

dx.doi.org/10.1021/jp211094n | *J. Phys. Chem. B* 2012, 116, 4024−4033

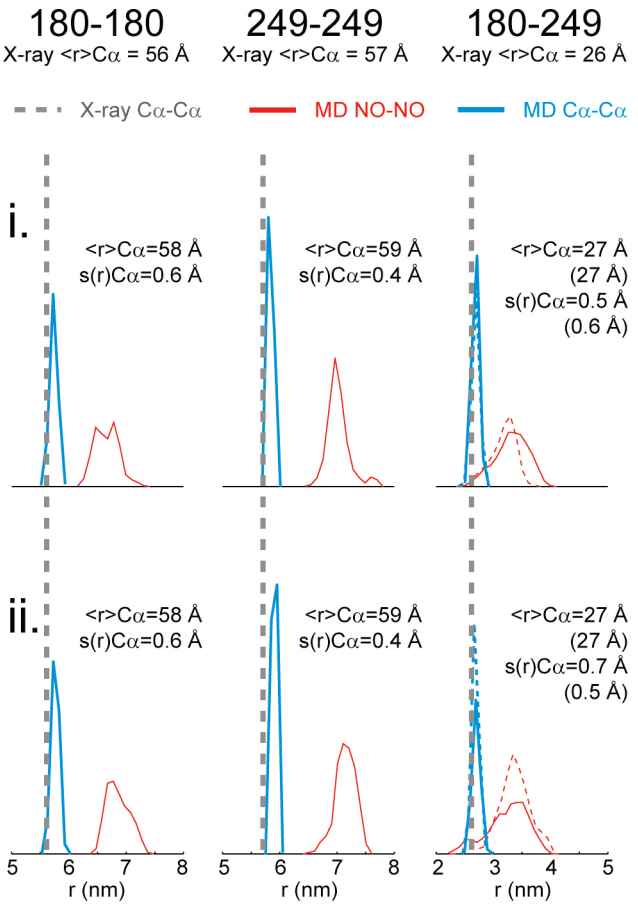

Figure 5. C_α–C_α distance distributions (blue) were extracted from the validated simulation results (red). The mean distances were compared to the C_α–C_α distance found in the crystal structure of the specific *Eco*RI–DNA complex (gray dashed line). The values from the crystal structure distances are listed above. The mean simulated C_α–C_α distance and standard deviation is listed by each distance distribution. The values in parentheses for the 180–249 distributions are those measured in the second monomer of *Eco*RI.

experiment and those that do not, the C_α–C_α distributions were fairly similar for all runs. The only exception to this occurred in runs that possessed an unstable rmsd and were found to have C_α–C_α distributions with larger standard deviations. This shows that MD simulations can distinguish spin label conformations even in the context of relatively invariant backbone distributions. Thus, favored spin label conformations can be extracted by comparing MD simulations with experimental data that provide multiple constraints.

Simulations were also carried out using the rotamer library approach implemented in the multiscale modeling of macromolecules (MMM) open-source package.[21,59] Spin label scans were performed at sites 180 and 249 in the specific *Eco*RI–DNA complex. Although the program successfully replicated the 180–180 experimental distance distribution, neither the 180–249 nor 249–249 distributions agreed with experiment. The distance distributions comparing the experimental data and the distributions obtained from the rotamer library are shown in Figure S5 in the Supporting Information. It can be seen in these fits that the 180–180 distribution agrees well with respect to the average distance as well as the standard deviation. However, the 249–249 distribution from the rotamer library possessed a lower average distance and a slightly broader distribution compared to experiment. The most significant difference arises from that of the 180–249 distribution in which the rotamer library predicted an average distance 0.6 nm lower than the experimental distribution. This indicates that, although the 180–180 simulation agreed with experiment, appropriate rotamers may not have been modeled that also agree with the 180–249 distribution.

Spin Label Dynamics and Conformers. In this work, the MD results provided insight into the dynamics and conformers of the spin label located at sites in different secondary structures: 180 (β-strand) and 249 (α-helix). Spin label dynamics and conformations were analyzed using those simulations that were determined to be consistent with the experimental distance distributions.

Polar plots, such as those used in previous works,[25,26,28] were constructed for each of the five dihedral angles that define the spin label side chain conformation (χ_1–χ_5). These plots are shown in Figure 6 for both sites 180 and 249. Each plot for a given dihedral angle displays the values sampled by that angle for both of the validated MD runs combined (runs **i** and **ii**). The radial distance from the center reflects the occupancy of that dihedral angle value throughout the portion of the simulation used for analysis (last 20 ns). In addition, the distribution about a value provides insight into the flexibility of that dihedral angle.

It can be seen from these polar plots that the dihedral angles sampled by sites 180 and 249 are similar to those found in the torsional potential energy surfaces constructed by Tombolato et al.[18] One exception to this is the value of χ_4 at site 180, where it samples a dihedral value of +110° in addition to the expected +75°. One can observe differences in the population of the dihedral angles sampled as well as the distribution about these angles between sites 180 and 249. The biggest difference arises between dihedral angles χ_1, χ_2, and χ_4. A significant example is seen in the χ_1 occupancy of the +65° conformation. At site 180, which resides on an edge β-strand, this χ_1 conformation is significantly sampled. However, at the α-helical site 249, this χ_1 conformation is infrequent. Similar trends are seen in values occupied by the χ_2 and χ_4 dihedral angles. Both the ±90° values of χ_3 are accessed at each site, and χ_5 is equally flexible and samples a variety of values at both sites.

Similar polar plots were constructed for the simulated results that did not agree with experiment (Figure S6, Supporting Information). These plots show a different pattern in both the dihedral angles that were sampled as well as in the the occupancies of the dihedral angles, compared to the runs that were able to replicate the experimental distance distributions. The most significant difference at site 180 is the decrease in the χ_1 = +65° conformer and an increase in $\chi_2 = \chi_4$ = 180°. The spin label conformation is extended when $\chi_2 = \chi_4$, leading to an increase in the average nitroxide–nitroxide distance. This is true for any χ_1 or χ_3 orientation. Thus, conformations of the spin label at site 180 where $\chi_2 = \chi_4$ are more likely to not agree with experiment due to a larger average distance. At site 249, the polar plots that did not agree with experiment show a significant increase of $\chi_2 = \chi_4$ = 180° as well as χ_4 = +75°. Similar to site 180, an increase in $\chi_2 = \chi_4$ conformers at site 249 could lead to average nitroxide–nitroxide distances larger than experiment. There are also changes in the χ_3 profile for both sites; however, the occupancy of χ_3 is influenced by the initial assignment of the conformation, and therefore no conclusions were drawn about changes in χ_3 between the different sets of fits. Comparison of the polar plots highlights the significance of

dx.doi.org/10.1021/jp211094n | J. Phys. Chem. B 2012, 116, 4024–4033

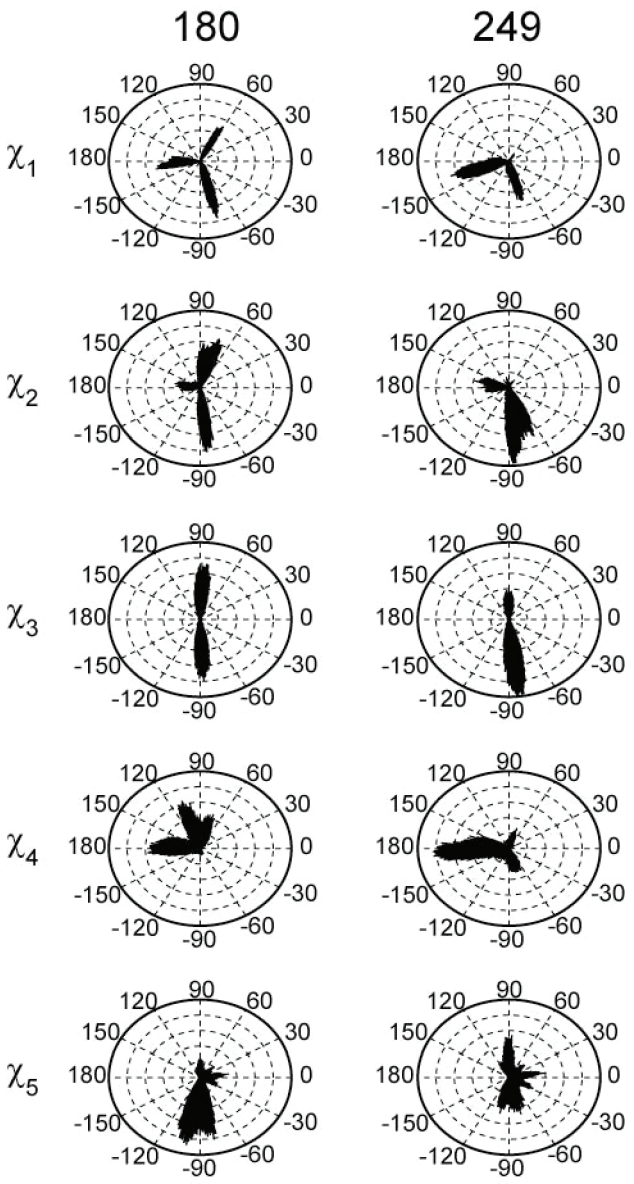

Figure 6. Polar plots illustrating the dihedral angle values sampled by the spin label at sites 180 and 249 for the simulations that agreed with experiment. The results of the two runs are combined in each of the plots for each site. The plots have been normalized with respect to the dihedral angle occupancy.

identifying and analyzing such validated simulation results because it exposes conformers that are sampled in MD runs that are not experimentally relevant.

No correlation was found between the starting rotamer used for the spin label and agreement with experiment. However, starting with different rotamers of the spin label does enhance the sampling of the spin-labeled location. For instance, although in each of the 10 runs the starting orientation of the spin label was the same in both monomers of the *Eco*RI complex, the two spin labels still sampled different conformers. By enhancing the conformers sampled throughout the simulation, the chance of identifying conformers that agree with experiment is increased.

The distribution and jumps about these dihedral angles provides insight into the dynamics of the spin label. The χ_4 and χ_5 polar plots show several dihedral angles sampled as well as broad distributions about these values. This indicates increased torsional oscillations and jumps about the two terminal angles of the spin label. These oscillations and jumps are also evident in the time-dependent trajectories of χ_4 and χ_5 (Figure S7 and S8, Supporting Information). The fast dynamics of χ_4 and χ_5 agrees with the previously proposed χ_4/χ_5 model of motion in which the main contributor to the spin label mobility has been proposed to arise from motion about the χ_4 and χ_5 dihedral angles.[36,37]

Conformers found in runs **i** and **ii** of the validated results were identified at sites 180 and 249, allowing comparison of the conformers sampled by the spin label at different secondary structures. To identify the conformers sampled from the simulated results, the dihedral angles were rounded to those found in the torsional potential energy profiles of the spin label.[18] The conformers identified are listed in Figure 7 along with a pictorial representation to visually demonstrate the difference in the conformers at each site. The conformers shown in Figure 7 were the highest occupied in runs **i** and **ii**. Due to the flexibility in the χ_5 angle, all possible values of χ_5 were considered when identifying the conformers.

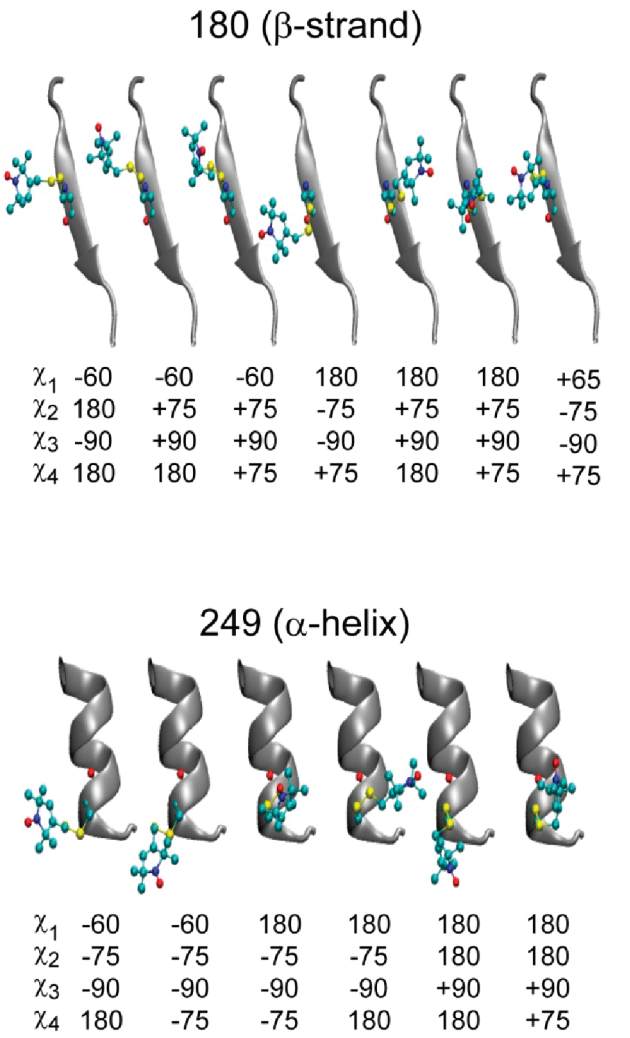

Figure 7. The significantly sampled conformers present in the validated simulations are shown for sites 180 and 249. Below the pictorial representations are the rounded dihedral angle values (χ_1–χ_4) for each conformation. All possible χ_5 values were considered in the identified conformers.

dx.doi.org/10.1021/jp211094n | *J. Phys. Chem. B* 2012, 116, 4024–4033

Using the CRBP, Lietzow and Hubbell suggested preferred geometries of several spin-labeled sites on interior and edge β-strands by CW-ESR analysis and manual variation of the spin label conformation built into the CRBP crystal structure.[40] From this work they proposed that edge strands, such as where 180 is located, favor [χ_1, χ_2] conformations of [+60, −60] and [+60, 180] (dihedral values as used by Hubbell and co-workers).[40] This is due to the non-hydrogen bonding (NHB) neighbor of the β-strand lying close to the spin label and therefore preventing the commonly observed [−60, −60] conformation. Indeed, the [−60, −60] conformer was rarely occupied in the validated MD results at site 180, but neither was the [+60, 180] conformation. The [+65, −75] conformer *was* observed, however. Other conformers were also observed such as [−60, +75], [−60, 180], and χ_1 = 180° conformers. These conformers may arise from the degree of strand twist in the β-strand or local side chain interactions at site 180. It was proposed that when the degree of strand twist increases, the residues will spread out and reduce side chain−spin label interactions.[40] In addition, different conformers of the spin label at 180 reside in close proximity to residues in the outer arm of *Eco*RI. For example, the [180, +75] conformer is positioned in close proximity to an asparagine residue on the adjacent β-strand, which is the NHB neighbor of site 180. As pointed out by Lietzow and Hubbell,[40] spin labels present on β-strands are expected to interact more with NHB neighbors that are β-branched residues, such as valine or isoleucine. It can be reasoned that because the NHB neighbor of site 180 is not β-branched, there exists little interaction between the two residues. Taken together with the strand twist present in the β-strand at site 180, alternative conformations of the spin label are possible.

As noted previously, most studies that have investigated spin label conformations and dynamics have been performed on α-helical sites. Although site 180 provides insight into the behavior of the spin label on a different secondary structure such as a β-strand, modeling on an α-helical motif, such as at site 249, provides a reference to compare these MD simulations with the work of others. Using X-ray crystallography, several preferred spin label conformers have been identified on solvent-accessible α-helical sites in T4 lysozyme. From these structures, the most preferred [χ_1, χ_2] conformations were found to be [−60, −60], [180, +60], and, to a lesser extent, [180, −60]. These conformers are also found to be energetically favorable in the DFT calculations performed by Warshaviak et al.[19] The [−60, −60] and [180, +60] spin label conformers are believed to be stabilized by the $S_\delta\cdots H-C_\alpha$ interaction of the spin label with the protein backbone.[11,19] In the [180, −60] conformation, the S_δ apparently interacts with the backbone C═O.[19] At site 249, two of these three preferred conformers were significantly sampled in the validated simulations: [−60, −75] and [180, −75]. Tombolato et al. and Sezer et al. both found the [−60, 180] conformer to be the most probable in their simulations on a polyalanine α-helix.[18,20] The [−60, 180] conformation was observed at site 249, however, not as significantly as in the works of Tombolato et al. and Sezer et al. Lastly, the [180, 180] conformer was also sampled at site 249. The [−60, −75], [180, −75], and [180,180] were also observed in the work of both Tombolato et al. and Sezer et al., however, to a lesser extent.

Hubbell and co-workers have shown that the [−60, 180] and [180, 180] conformers are sterically allowed at α-helical sites (i.e., those modeled in T4 lysozyme), but are rarely observed in the crystal structures. For example, the [−60, 180] conformer has been observed only once, and that at a crystal contact site.[14] It is proposed that these conformers are not stabilized by the $S_\delta\cdots H-C_\alpha$ interaction, and thus their χ_2 angles are less constrained, so that mobility or distribution among conformers produces weak crystallographic electron densities. Such disorder is not observed in the solution CW spectra.[11] Additionally, the [−60,180] conformation was found to possess the highest relative energy in the recent DFT calculations.[19] The MD force field used in this work lacks the appropriate details, such as polarizability, to observe the possible lone pair interaction between the spin label S_δ atom and the hydrogen from the backbone $H-C_\alpha$. Thus, these conformers may be less probable in experiment due to the stabilization of other conformers, i.e., [−60, −60], [180, +60], and [180, −60], by this interaction. Such discrepancies between simulation and experiment expose the limitations of the current simulation techniques. Even if the simulations are extended or general sampling is increased, the spin label may still sample conformers that are less likely to be observed experimentally. Thus, agreement between the MD results and experiment may not always be plausible, even if the simulations are carried out for much longer time scales. Ultimately, only the conformers that agree with the experimental constraints should be considered.

Different preferred conformers were occupied by the spin label present on different secondary structures. Site 180, present on an edge β-strand, was the only site where the χ_1 = +65° conformer was significantly sampled. It has been mentioned that such a conformation of the χ_1 dihedral angle is sterically forbidden in nearly all α-helical sites,[11] and in fact this conformer was rarely occupied at the 249 site. Interestingly, no one preferred conformer was the same for site 180 and 249. This underscores the sensitivity of the spin label to the secondary structural location.

Broad Utility of Approach. We have shown in this work the value of using MD simulations to model the spin label conformer and dynamics at two different secondary structures. Insight gained into the behavior of the spin label on a β-strand is significant due to the limited amount of information that exists on the behavior of the spin label in β-strands or β-sheets. In addition, we have demonstrated the need to extend MD simulations to longer time scales (>10 ns) to ensure backbone equilibration of the system as well as to effectively sample the spin label conformers. We have also shown that the use of correlated experimental distance constraints can provide strict criteria for agreement between simulation and experiment, and thus for identifying the most probable conformers in solution. Since the favored conformations of the spin label are likely to depend primarily on highly local features of its secondary structure environment, these favored conformations can then be used to deconvolute positional distributions of the spin label from positional distributions of the backbone. The potential utility of our approach is thus in establishing the favored spin label conformation for a particular location in a protein. This information can then be used to extract differences in backbone distributions when comparing complexes of the same protein (whose secondary structure should often be conserved) with different ligands or under different solution conditions. This work underscores the need for new methods to simulate spin label packing and conformations in different systems and at different secondary structures. Methods such as the rotamer

dx.doi.org/10.1021/jp211094n | J. Phys. Chem. B 2012, 116, 4024−4033

search[33,34,39] and rotamer library[21−23] provide alternative means to account for spin label conformational distributions.

CONCLUSIONS

ESR-DEER experiments on proteins yield distance distributions that convolute the effects of backbone positions and motions with preferred conformations and dynamics of the spin label moieties. These factors can be deconvoluted by MD simulation, provided that the simulations accurately reproduce the experimental ESR-DEER data. This we have done successfully for spin-labeled sites 180 and 249 of the specific *Eco*RI−DNA complex, also allowing us to compare spin label behaviors when located on a β-strand or an α-helix. These simulation studies enhance our understanding of the behavior of spin labels in proteins and thus expand the ability of ESR spectroscopy to contribute to knowledge of protein structure and function.

ASSOCIATED CONTENT

Supporting Information

Distance distributions and rmsd trajectories for runs **iii**, **iv**, and **vi**−**x**, raw 249−249 DEER data, trimer of dimers modeling, rotamer library distance distributions, polar plots for runs **v**−**x**, and dihedral angle trajectories for runs **i** and **ii** at sites 180 and 249. This material is available free of charge via the Internet at http://pubs.acs.org.

AUTHOR INFORMATION

Corresponding Author

*Phone: (412) 624-8680. Fax: (412) 624-8611. E-mail: sksaxena@pitt.edu.

Notes

The authors declare no competing financial interest.

ACKNOWLEDGMENTS

The MD and ESR studies were supported by a National Science Foundation (MCB 0842956) grant to S.S. and L.J.-J. Generation of mutant proteins and spin labeling were supported by a National Institutes of Health MERIT (5R37-GM029207) grant to L.J.-J. The simulations were also supported by the NSF through TeraGrid resources provided by the Pittsburgh Supercomputing Center under Grant Number TG-CHE100114 and the University of Pittsburgh Center for Simulation and Modeling. J.L.S. thanks Mike Yonkunas for helpful instruction on the MD simulations and Dan Zuckerman for his insight on the manuscript.

REFERENCES

(1) Fanucci, G. E.; Cafiso, D. S. *Curr. Opin. Struct. Biol.* **2006**, *16*, 644−653.
(2) Columbus, L.; Hubbell, W. L. *Trends Biochem. Sci.* **2002**, *27*, 288−295.
(3) Milov, A. D.; Ponomarev, A. B.; Tsvetkov, Y. D. *Chem. Phys. Lett.* **1984**, *110*, 67−72.
(4) Martin, R. E.; Pannier, M.; Diederich, F.; Gramlich, V.; Hubrich, M.; Spiess, H. W. *Angew. Chem., Int. Ed.* **1998**, *37*, 2833−2837.
(5) Margraf, D.; Bode, B. E.; Marko, A.; Schiemann, O.; Prisner, T. F. *Mol. Phys.* **2007**, *105*, 2153−2160.
(6) Pornsuwan, S.; Bird, G.; Schafmeister, C. E.; Saxena, S. *J. Am. Chem. Soc.* **2006**, *128*, 3876−3877.
(7) Jeschke, G.; Sajid, M.; Schulte, M.; Ramezanian, N.; Volkov, A.; Zimmermann, H.; Godt, A. *J. Am. Chem. Soc.* **2010**, *132*, 10107−10117.
(8) Pornsuwan, S.; Schafmeister, C. E.; Saxena, S. *J. Phys. Chem. C* **2008**, *112*, 1377−1384.
(9) Godt, A.; Schulte, M.; Zimmermann, H.; Jeschke, G. *Angew. Chem., Int. Ed.* **2006**, *45*, 7560−7564.
(10) Freed, D. M.; Horanyi, P. S.; Wiener, M. C.; Cafiso, D. S. *Biophys. J.* **2010**, *99*, 1604−1610.
(11) Fleissner, M. R.; Cascio, D.; Hubbell, W. L. *Protein Sci.* **2009**, *18*, 893−908.
(12) Guo, Z.; Cascio, D.; Hideg, K.; Hubbell, W. L. *Protein Sci.* **2008**, *17*, 228−239.
(13) Guo, Z.; Cascio, D.; Hideg, K.; Kalai, T.; Hubbell, W. L. *Protein Sci.* **2007**, *16*, 1069−1086.
(14) Langen, R.; Oh, K. J.; Cascio, D.; Hubbell, W. L. *Biochemistry* **2000**, *39*, 8396−8405.
(15) Gruene, T.; Cho, M.-K.; Karyagina, I.; Kim, H.-Y.; Grosse, C.; Giller, K.; Zweckstetter, M.; Becker, S. *J. Biomol. NMR* **2011**, *49*, 111−119.
(16) Kroncke, B. M.; Horanyi, P. S.; Columbus, L. *Biochemistry* **2010**, *49*, 10045−10060.
(17) Freed, D. M.; Khan, A. K.; Horanyi, P. S.; Cafiso, D. S. *Biochemistry* **2011**, *50*, 8792−8803.
(18) Tombolato, F.; Ferrarini, A.; Freed, J. H. *J. Phys. Chem. B* **2006**, *110*, 26248−26259.
(19) Warshaviak, D. T.; Serbulea, L.; Houk, K. N.; Hubbell, W. L. *J. Phys. Chem. B* **2011**, *115*, 397−405.
(20) Sezer, D.; Freed, J. H.; Roux, B. *J. Phys. Chem. B* **2008**, *112*, 5755−5767.
(21) Polyhach, Y.; Bordignon, E.; Jeschke, G. *Phys. Chem. Chem. Phys.* **2011**, *13*, 2356−2366.
(22) Hilger, D.; Polyhach, Y.; Jung, H.; Jeschke, G. *Biophys. J.* **2009**, *96*, 217−225.
(23) Hilger, D.; Polyhach, Y.; Padan, E.; Jung, H.; Jeschke, G. *Biophys. J.* **2007**, *93*, 3675−3683.
(24) Oganesyan, V. S. *Phys. Chem. Chem. Phys.* **2011**, *13*, 4724−4737.
(25) Beier, C.; Steinhoff, H.-J. *Biophys. J.* **2006**, *91*, 2647−2664.
(26) Budil, D. E.; Sale, K. L.; Khairy, K. A.; Fajer, P. G. *J. Phys. Chem. A* **2006**, *110*, 3703−3713.
(27) Sezer, D.; Freed, J. H.; Roux, B. *J. Am. Chem. Soc.* **2009**, *131*, 2597−2605.
(28) DeSensi, S. C.; Rangel, D. P.; Beth, A. H.; Lybrand, T. P.; Hustedt, E. J. *Biophys. J.* **2008**, *94*, 3798−3809.
(29) Ding, F.; Layten, M.; Simmerling, C. *J. Am. Chem. Soc.* **2008**, *130*, 7184−7185.
(30) Borovykh, I. V.; Ceola, S.; Gajula, P.; Gast, P.; Steinhoff, H.-J.; Huber, M. *J. Magn. Reson.* **2006**, *180*, 178−185.
(31) Ranaldi, S.; Belle, V.; Woudstra, M.; Bourgeas, R.; Guigliarelli, B.; Roche, P.; Vezin, H.; Carriére, F.; Fournel, A. *Biochemistry* **2010**, *49*, 2140−2149.
(32) Sale, K.; Sar, C.; Sharp, K. A.; Hideg, K.; Fajer, P. G. *J. Magn. Reson.* **2002**, *156*, 104−112.
(33) Fajer, M. I.; Sale, K. L.; Fajer, P. G. In *ESR Spectroscopy in Membrane Biophysics*; Hemminga, M. A., Berliner, L. J., Eds.; Springer: New York, 2007; Vol. *27*, pp 254−257.
(34) Fajer, M. I.; Li, H.; Yang, W.; Fajer, P. G. *J. Am. Chem. Soc.* **2007**, *129*, 13840−13846.
(35) Sen, K. I.; Logan, T. M.; Fajer, P. G. *Biochemistry* **2007**, *46*, 11639−11649.
(36) Mchaourab, H. S.; Lietzow, M. A.; Hideg, K.; Hubbell, W. L. *Biochemistry* **1996**, *35*, 7692−7704.
(37) Columbus, L.; Kalai, T.; Jeko, J.; Hideg, K.; Hubbell, W. L. *Biochemistry* **2001**, *40*, 3828−3846.
(38) Metropolis, N.; Rosenbluth, A. W.; Rosenbluth, M. N.; Teller, A. H. *J. Chem. Phys.* **1953**, *21*, 1087−1092.
(39) Li, H.; Fajer, M.; Yang, W. *J. Chem. Phys.* **2007**, *126*, 024106.
(40) Lietzow, M. A.; Hubbell, W. L. *Biochemistry* **2004**, *43*, 3137−3151.
(41) Kuo, W.; Herrick, D. Z.; Ellena, J. F.; Cafiso, D. S. *J. Mol. Biol.* **2009**, *387*, 284−294.

(42) Lai, A. L.; Huang, H.; Herrick, D. Z.; Epp, N.; Cafiso, D. S. *J. Mol. Biol.* **2011**, *405*, 696−706.
(43) Flores Jiménez, R. H.; Freed, D. M.; Cafiso, D. S. *J. Phys. Chem. B* **2011**, *115*, 14822−14830.
(44) Lesser, D. R.; Kurpiewski, M. R.; Jen-Jacobson, L. *Science* **1990**, *250*, 776−786.
(45) Sapienza, P. J.; dela Torre, Crystal A.; W. H., M. IV; Jana, S. V.; Jen-Jacobson, L. *J. Mol. Biol.* **2005**, *348*, 307−324.
(46) Grigorescu, A.; Horvath, M.; Wilkosz, P. A.; Chandrasekhar, K.; Rosenberg, J. M. In *Restriction Endonucleases*; Pingoud, A., Ed.; Springer-Verlag: Berlin Heidelberg, 2004; Vol. *14*, pp 137−177.
(47) Kim, Y.; Grable, J. C.; Love, R.; Greene, P. J.; Rosenberg, J. M. *Science* **1990**, *249*, 1307−1309.
(48) Sapienza, P. J.; Rosenberg, J. M.; Jen-Jacobson, L. *Structure* **2007**, *15*, 1368−1382.
(49) Stone, K. M.; Townsend, J. E.; Sarver, J.; Sapienza, P. J.; Saxena, S.; Jen-Jacobson, L. *Angew. Chem., Int. Ed.* **2008**, *120*, 10346−10348.
(50) Jen-Jacobson, L.; Kurpiewski, M.; Lesser, D.; Grable, J.; Boyer, H. W.; Rosenberg, J. M.; Greene, P. J. *J. Biol. Chem.* **1983**, *258*, 14638−14646.
(51) Humphrey, W.; Dalke, A.; Schulten, K. *J. Mol. Graphics* **1996**, *14.1*, 33−38.
(52) Brooks, B. R.; Bruccoleri, R. E.; Olafson, B. D.; States, D. J.; Swaminathan, S.; Karplus, M. *J. Comput. Chem.* **1983**, *4*, 187−217.
(53) Mackerell, A. D.; Feig, M.; Brooks, C. L. *J. Comput. Chem.* **2004**, *25*, 1400−1415.
(54) Phillips, J. C.; Braun, R.; Wang, W.; Gumbart, J.; Tajkhorshid, E.; Villa, E.; Chipot, C.; Skeel, R. D.; Kale, L.; Schulten, K. *J. Comput. Chem.* **2005**, *26*, 1781−1802.
(55) Dylla-Spears, R.; Townsend, J. E.; Sohn, L. L.; Jen-Jacobson, L.; Muller, S. J. *Anal. Chem.* **2009**, *81*, 10049−10054.
(56) Jeschke, G.; Chechik, V.; Ionita, P.; Godt, A.; Zimmermann, H.; Banham, J.; Timmel, C.; Hilger, D.; Jung, H. *Appl. Magn. Reson.* **2006**, *30*, 473−498.
(57) van Gunsteren, W. F.; Dolenc, J.; Mark, A. E. *Curr. Opin. Struct. Biol.* **2008**, *18*, 149−153.
(58) Grigorescu, A. Ph.D. Thesis, University of Pittsburgh, 2003.
(59) ETH Zurich, EPR Research Group, Software; http://www.epr.ethz.ch/sofware/index (accessed August 2010).